ISBN: 978-3-95450-227-1 ISSN: 2673-5490 doi:10.18429/JACoW-IPAC2022-TUPOPT059

MACHINE LEARNING METHODS FOR CHROMATICITY CONTROL AT THE 1.5 GeV SYNCHROTRON LIGHT SOURCE DELTA

D. Schirmer*, A. Althaus, T. Schüngel
Center for Synchrotron Radiation (DELTA), TU Dortmund University, Germany

Abstract

In the past, the chromaticity values at the DELTA electron storage ring were manually adjusted using 15 individual sextupole power supply circuits, which are combined into 7 magnet families. To automate and optimize the time-consuming setting process, various machine learning approaches were investigated. For this purpose, simulations were first performed using a storage ring model and the performance of different neural networks based models was compared. Subsequently, the neural networks were trained with experimental data and successfully implemented for chromaticity correction in real accelerator operation.

INTRODUCTION

DELTA is a 1.5–GeV electron storage ring facility operated by the TU Dortmund University as a synchrotron light source [1] and as a facility for ultrashort pulses in the VUV and THz regime [2, 3].

In recent years, different machine learning (ML) based projects have been investigated to support automated monitoring and operation of the DELTA electron storage ring facility [4]. This includes self-regulating global and local orbit correction of the stored electron beam [5, 6] and a betatron tune feedback [7]. In addition, a ML-based electron transfer rate (injection) optimization is in preparation [8].

So far, the storage ring chromaticity values have been adjusted empirically based on experience. The setting of desired target values can only be achieved by time-consuming trial and error. For this reason, ML-based algorithms for automated chromaticity adjustment were investigated, very similar to the already implemented ML-based betatron tunes control [7].

In previous studies, the workflow was successfully simulated on a storage ring model. Therefore, the correlation between sextupole magnet strength changes and the related chromaticity shifts was investigated. In this case, the magnets were grouped via software in four horizontal and three vertical focusing families. Here, clear correlations were identified during training of conventional 3-layered feed-forward neural networks (NNs), without any over- or underfitting issues. Afterwards, the trained NN-based models were able to match the chromaticity to any desired value in the simulated storage ring. Some results are summarized in [4] and [8].

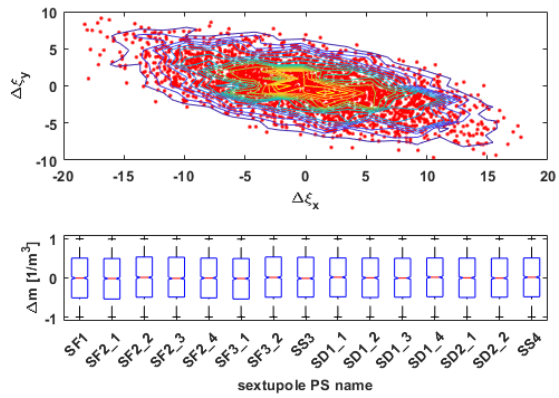

Figure 1: Distribution of 3000 chromaticity shifts (top) invoked by uniformly randomized strength variations of 15 independent sextupole power supplies (PS) circuits (bottom). The data are obtained by AT optics simulations based on a DELTA storage ring lattice model.

ML-BASED SIMULATED CHROMATICITY CONTROL

To increase the degree of freedom for automated chromaticity control, we repeated the pre-studies, but now utilizing all 15 sextupole PS circuits individually. A detailed lattice model of the DELTA storage ring served as the basis for x,y-coupled optics and chromaticity (ξ_x, ξ_y) computations within the Accelerator Toolbox (AT) framework [9, 10]. To acquire suitable ML training data, the sextupole strengths were randomly varied for all 15 PS individually and for each strength change setting, the associated chromaticity shifts were calculated. Fig. 1 visualizes the corresponding AT simulation results.

These labelled data pairs (strength variations and chromaticity shifts) were used for supervised training of multilayered NNs. The NNs serve as surrogate models for the chromaticity determination, which afterwards are applied to automatically adjust and control the chromaticity values.

Fig. 2 illustrates a sample application for a simulated chromaticity matching run performed with a 3-layered NN which has been trained by scaled conjugate gradient (scg) back-propagation [11] applying the data depicted in Fig. 1. The natural chromaticity ($\xi_x = -21$, $\xi_y = -8$) which occurs with all sextupoles switched off (0. iteration) can be adjusted to full chromaticity compensated values (4. iteration, $\xi_x = \xi_y = 0$) by the ML-based control loop. The step size (number of iterations) depends mainly on the granularity ($\Delta\xi_{x,y}$) of

* detlev.schirmer@tu-dortmund.de

ISBN: 978-3-95450-227-1 ISSN: 2673-5490 doi:10.18429/JACoW-IPAC2022-TUPOPT059

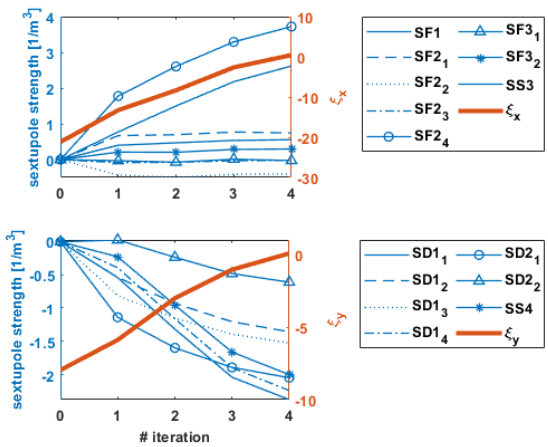

Figure 2: Example for verification of NNs trained by simulated data (see Fig. 1) and applied to the DELTA storage ring model. The desired target values for compensated chromaticity (goal: $\xi_x = \xi_y = 0$) were reached in 4 iterative steps (red curves) starting at the setting for natural chromaticity ($\xi_x = -21$, $\xi_y = -8$, sextupoles switched off). The corresponding sextupole strength adaptions are shown in blue lines. In total, 15 individual power supplies (PS) are available to operate 7 sextupole magnet families. They are grouped in four horizontal (top: SF1, SF2, SF3, SS3) and three vertical (bottom: SD1, SD2, SS4) focusing families. The indices number the individual PS circuits.

the training data (see Fig. 1). During the magnet settings, all strengths remain below the maximum limit of 4 $[1/m^3]$ and single PS circuits adjust slightly differently in some cases.

REAL MACHINE OPERATION

A similar approach was adapted for real machine operation. Here too, all seven sextupole families were split into 15 individual PS circuits. For chromaticity determination in real storage ring operation, the cavity radiofrequency (RF) must be shifted and then the tune shifts ΔQ are determined via a FFT spectrum from turn-by-turn orbit data at a dedicated beam position monitor (BPM). See Fig. 3 as an example. With $\Delta Q = \xi \cdot \Delta p/p$ follows for the chromaticity $\xi = \Delta Q \cdot p/\Delta p = -\alpha_c h \Delta f_\beta / \Delta f_{\mathrm{RF}}$. Δf_{RF} corresponds to changes of the cavity radiofrequency, Δf_β is the measured betatron frequency shift, h is the harmonic number and the momentum compaction factor $\alpha_c = (\Delta L/L)/(\Delta p/p)$ relates the relative orbit path length change $\Delta L/L$ to the relative momentum change $\Delta p/p$. The precision of the FFT method is limited to plus or minus half a spectrum bin, which is in our case ±2.5 kHz, corresponding to a fast tune measurement resolution of $\pm 1 \cdot 10^{-3}$ [12]. To enable rapid data acquisition (DAQ) on the one hand but to avoid beam losses on the other hand the RF shift was stepwise adjusted to a limit of ±6 kHz. This corresponds to a maximum tune shift of approximately $\pm 1 \cdot 10^{-2}$ and results finally in a limited chromaticity measurement precision of about 0.2 (see the top of Fig. 4 and Fig. 5).

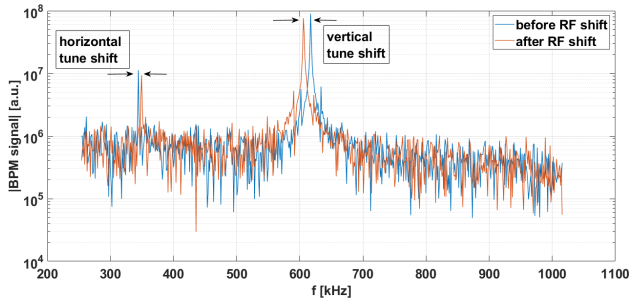

Figure 3: FFT beam spectrum from turn-by-turn orbit data recorded at a dedicated BPM. Before (blue) and after (red) cavity radiofrequency (RF) variation. The horizontal and vertical chromaticities are calculated by determining the betatron tune peak shifts induced by the cavity RF variation.

In dedicated data mining shifts a Python/EPICS-based DAQ-script varied randomly individual PS current values related to a nominal sextupole reference setting and then measured the corresponding chromaticity changes ($\Delta\xi_{x,y}$). To avoid beam losses the magnet current variations were limited to +/-15% (uniformly and Gaussian distributed) and were additionally extracted if sextupole magnet hardware limits were exceeded. Due to the limited chromaticity measurement resolution, the values pile on a fixed $\Delta\xi_{x,y}$-grid. The histogram plot (see Fig. 4) shows the number of measurements with the same chromaticity shift per bin. The measurement for each data pattern took about 20 seconds. After data cleaning of mismeasurements, we obtained 2749 data patterns which were again used for training of classical multi-layered, fully-connected feed-forward NNs. The regression results obtained from the application of a trained NN are shown exemplarily in Fig. 5. In this example the validation regres-

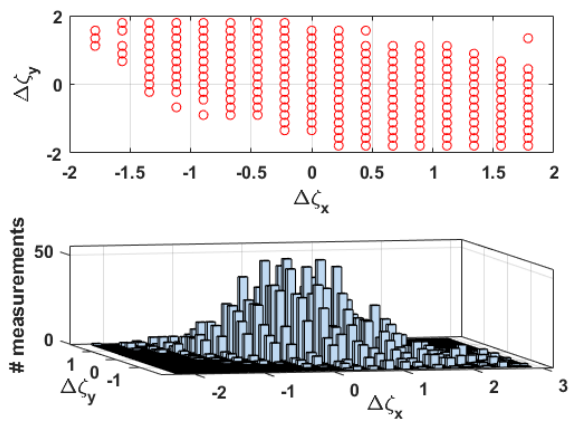

Figure 4: Distribution of 2749 measured chromaticity shifts (cleaned data) invoked by uniformly and Gaussian randomized strength variations of 15 independent sextupole power supplies circuits (bottom). Due to granularity constrictions of the chromaticity measurements, all values are distributed on a resolution-limited grid (top).

ISBN: 978-3-95450-227-1 ISSN: 2673-5490 doi:10.18429/JACoW-IPAC2022-TUPOPT059

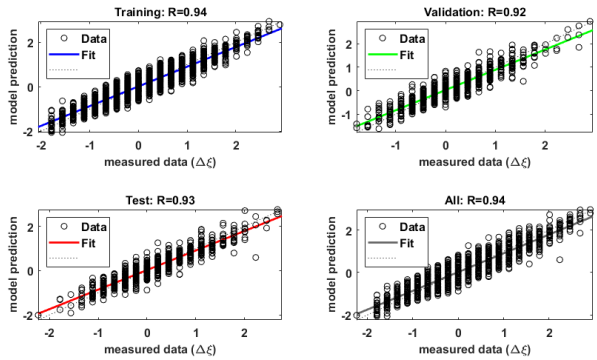

Figure 5: Comparison between measured data and model predictions of a scaled conjugate gradient back-propagation (scg, [11]) trained NN-based surrogate model. The complete set of 2749 experimental data patterns was divided into 70% for pure network training and 15% of the data are applied as "unseen" data sets for validation and test, respectively. The R-values rate the correlation quality between experimental data and NN model prediction.

sion coefficient is calculated to R = 0.92, indicating high modelling capabilities for chromaticity predictions. To make a prediction on how to improve the chromaticity a weighting-function-driven optimization algorithm, like Bayesian optimization using Gaussian Processes (GP) [13–15], scored the output of the NN-based surrogate models. If required, the score function can also consider additional boundary conditions, e. g. maximum sextupole strength, beam lifetime or PS current stepsize. Afterwards, the optimization results (new predicted sextupole strength settings) are applied to the storage ring. Then the associated chromaticity corrections are experimentally measured (see above), giving new start values for the next optimization iteration until the desired target chromaticity is reached. An example of such a chromaticity matching procedure is shown in Fig. 6 (red curves). In this case, 10 steps were necessary to obtain the target values ($\xi_x = \xi_y = 0$) starting at $\xi_x = -10$, $\xi_y = -4.4$, which were obtained with sextupole magnets operated at half nominal strength. The maximum and minimum step sizes depend mainly on the $\Delta\xi_{x,y}$-granularity of the training data sets. The corresponding sextupole strength changes are also depicted in Fig. 6 (blue curves). This showed, that the originally identical family values split into different values during the matching run. This reflects the asymmetry of the real machine optics. For comparison, the same optimization was carried out, but now while maintaining the fixed sextupole family membership (see Fig. 7). In both examples, the desired chromaticity ($\xi_x = \xi_y = 0$) was achieved in about 10 iterations without exceeding the technical current limit of 15 A. More detailed studies are currently being conducted.

SUMMARY AND OUTLOOK

It has been shown that classical machine learning methods like conventional feed-forward neural networks are appropriate for chromaticity control in simulation as well as in the real storage ring operation. Splitting the PS-families into individual PS circuits has increased the flexibility to approach arbitrary chromaticity settings. Further studies need to be conducted to understand the different correction behaviour in simulation and the real storage ring operation, respectively. Work is currently in preparation to implement the entire ML-workflow on a dedicated ML-server applying software container (Docker [16]) techniques. In the future ML-based methods could additionally be extended to optimize the sextupole settings with respect to dynamic aperture and thus to increase the stored beam life time.

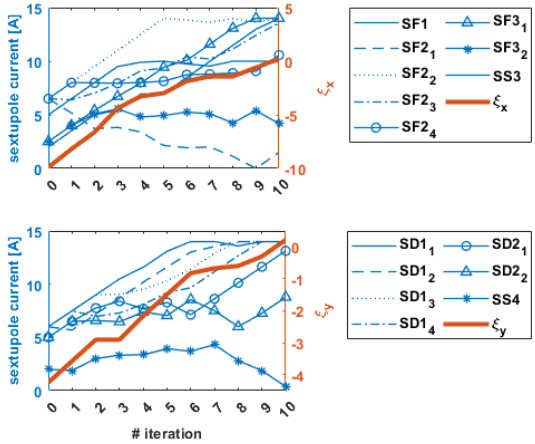

Figure 6: Example application to test NNs trained by experimental data (see Fig. 4) and applied to the real storage ring. The desired target values for compensated chromaticity (target: $\xi_x = \xi_y = 0$) were reached in 10 iterative steps starting with chromaticity values of $\xi_x = -10$ and $\xi_y = -4.4$.

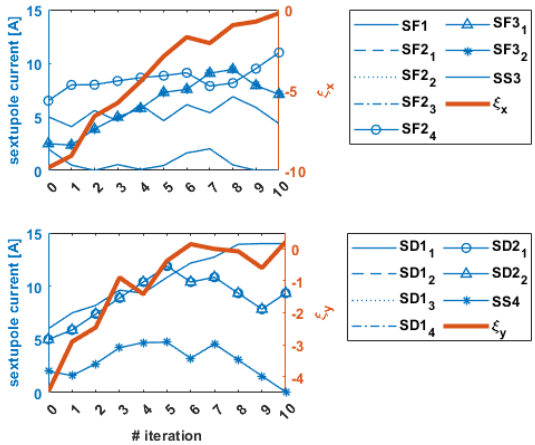

Figure 7: The same optimization run as shown in Fig. 6. Here with fixed magnet family affiliations, grouped in 4 horizontally and 3 vertically focussing PS circuits. Therefore, the lines of the indexed sextupole PS circuits lie on top of each other.

ISBN: 978-3-95450-227-1 ISSN: 2673-5490 doi:10.18429/JACoW-IPAC2022-TUPOPT059

REFERENCES

[1] M. Tolan, T. Weis, C. Westphal, and K. Wille, "DELTA: Synchrotron light in nordrhein-westfalen", *Synchrotron Radiation News 16(2)*, 9–11, (2003). doi:10.1080/08940880308603005

[2] S. Khan *et al.*, "Coherent Harmonic Generation at DELTA: A New Facility for Ultrashort Pulses in the VUV and THz Regime", in *Synchrotron Radiation News 24(5)*, 18–23, (2011). doi:10.1080/08940886.2011.618092

[3] S. Khan *et al.*, "Generation of Ultrashort and Coherent Synchrotron Radiation Pulses at DELTA", *Synchrotron Radiation News 26(3)*, 25–29, (2013). doi:10.1080/08940886.2013.791213

[4] D. Schirmer, A. Althaus, S. Hüser, S. Khan, T. Schüngel, "Machine learning projects at the 1.5–GeV synchroton light source DELTA", in *Proc. of 18th Int. Conf. on Accelerator and Large Experimental Physics Control Systems (ICALEPCS'21)*, Shanghai, China, 2021, pp. 631–635. doi:10.18429/JACoW-ICALEPCS2021-WEPV007

[5] D. Schirmer, "Orbit Correction with Machine Learning Techniques at the Synchrotron Light Source DELTA", in *Proc. of 17th Int. Conf. on Accelerator and Large Experimental Physics Control Systems (ICALEPCS'19)*, New York, USA, 2019, pp. 1426–1430. doi:10.18429/JACoW-ICALEPCS2019-WEPHA138

[6] D. Schirmer, "A Machine Learning Approach to Electron Orbit Control at the 1.5-GeV Synchrotron Light Source DELTA", presented at the 13th International Particle Accelerator Conf. (IPAC'22), Bangkok, Thailand, Jun. 2022, paper TUPOPT058, this conference.

[7] D. Schirmer, "Machine learning applied to automated tunes control at the 1.5 GeV synchrotron light source DELTA", in *Proc. of 12th Int. Particle Accelerator Conf. (IPAC'21)*, Campinas, SP, Brazil, 2021, pp. 3379–3382. doi:10.18429/JACoW-IPAC2021-WEPAB303

[8] D. Schirmer, A. Althaus, S. Hüser, S. Khan, T. Schüngel, "New machine learning projects at DELTA", in *17th DELTA Annual Report 2021*, pp. 3–4, Dortmund, Germany, November 2021. https://www.delta.tu-dortmund.de/cms/Medienpool/User_Reports/DELTA_User_Report_2021.pdf

[9] Accelerator Toolbox (AT), http://atcollab.sourceforge.net/index.html.

[10] A. Terebilo, "Accelerator Modeling with Matlab Accelerator Toolbox", in *Proc. of 19th Particle Accelerator Conference (PAC'01)*, Chicago, USA, 2001, pp. 3203–3205. doi:10.1109/PAC.2001.988056

[11] Møller, M. F., "A scaled conjugate gradient algorithm for fast supervised learning", Neural Networks 6(4), 525-–533, 1993.

[12] P. Hartmann, J. Fürsch, R. Wagner, T. Weis, and K. Wille, "Kicker Based Tune Measurement for DELTA", in *Proc. of 8th European Workshop on Beam Diagnostics and Instrumentation for Particle Accelerators (DIPAC'07)*, Venice, Italy, 2007, pp. 277–279.

[13] C. E. Rasmussen and C. Williams, "Gaussian processes for machine learning", MIT Press, Cambridge, Mass., ISBN 9780262182539, 2005.

[14] https://scikit-optimize.github.io/stable/modules/generated/skopt.gp_minimize.html

[15] J. H. Snoek, H. Larochelle, R. P. Adams, "Practical Bayesian Optimization of Machine Learning Algorithms", https://doi.org/10.48550/arXiv.1206.2944, 2012.

[16] https://www.docker.com